Estimation of the Kelvin Wave Contribution to the Semiannual Oscillation

MATTHEW H. HITCHMAN AND CONWAY B. LEOVY

Department of Atmospheric Sciences, University of Washington, Seattle, Washington

(Manuscript received 11 June 1987, in final form 16 November 1987)

ABSTRACT

The behavior of Kelvin waves in the equatorial middle atmosphere is investigated with the use of daily mapped temperatures derived from the Limb Infrared Monitor of the Stratosphere (LIMS) experiment. Diagrams of wave activity per unit mass and wave activity flux density concisely illustrate bulk properties of Kelvin waves and facilitate tracing of packets to source times near the tropopause. Kelvin wave packets of different zonal wavenumbers propagate separately and appear to be forced separately. During the LIMS data period (25 October 1978–28 May 1979) two Kelvin wave regimes are found. Packets of wave one, wave two, or wave three Kelvin waves occur at irregular intervals prior to April. During April and May a nearly continuous upward flux of wave one activity dominates.

For very tall Kelvin waves the observed dependence of vertical wavelength on zonal wind is weaker than predicted by the slowly-varying theory for internal gravity waves. However, most properties of the observed waves are consistent with slowly-varying theory, and the zonal mean body force per unit mass due to Kelvin waves is estimated from observed temperatures and application of the WKBJ approximation. Both a flux convergence and radiative damping formulation yield westerly wave driving which is smaller than that required to satisfy the zonal momentum budget. A comparison of the residual of terms in the zonal momentum equation, estimated from LIMS data, with gravity wave driving, estimated by Lindzen's breaking parameterization, suggests that gravity waves may contribute significantly to the equatorial stratopause semiannual oscillation.

1. Introduction

Over the past twenty years evidence has been accumulating that the Kelvin wave plays a significant role in generating westerlies in the equatorial middle atmosphere (Wallace and Kousky 1968; Holton and Lindzen 1968; Hirota 1978; Dunkerton 1979). It is of considerable interest to determine this contribution quantitatively. The most detailed and complete observations of both Kelvin waves and the mean state come from the recent Limb Infrared Monitor of the Stratosphere (LIMS) experiment (Gille and Russell 1984; Salby et al. 1984). The observed behavior of Kelvin wave packets closely resembles results from a quasi-linear two dimensional gravity wave model (Coy and Hitchman 1984). In this study we employ WKBJ theory of gravity waves in making estimates of Kelvin wave driving based on daily synoptic values of LIMS temperature for Kelvin zonal waves one, two, and three.

The mapped temperature data used here are described in Hitchman and Leovy (1986, hereafter HL). Data precision is believed to be better than 0.5 K (Gille et al. 1984). Features with amplitudes larger than 2 K and vertical wavelengths exceeding 7 km should be represented in this data set. Errors in our estimates of Kelvin wave driving can arise from departures of actual wave behavior from idealized theory. In section 2 the slowly-varying theory for gravity waves is presented and expressions for evaluating wave driving from the available data are derived. Observed wave behavior is then compared with theory in section 3 and an assessment of probable errors in the wave driving estimates is given. Several interesting bulk properties of Kelvin waves are observed in the LIMS record. Implications for theories of Kelvin wave forcing are also discussed in section 3.

It is now believed that the equatorial middle atmosphere is driven primarily by waves propagating from the tropical and extratropical troposphere. Strong semiannual variations in the zonal mean state occur in the altitude range 30–90 km over the equator. Largest amplitudes in zonal wind ($\sim$30 m s^{-1}) occur near the mesopause ($\sim$80 km) and stratopause ($\sim$50 km), with very small amplitudes near 65 km (Hirota 1978; Hamilton 1982). The likelihood of separate sequences of forcing mechanisms has motivated distinguishing the mesopause and stratopause semiannual oscillations (Dunkerton 1982). The LIMS data allow examination of the region $\sim$ 20–70 km. This analysis therefore applies chiefly to the stratopause semiannual oscillation (hereafter SAO), but also extends into the lower mesosphere.

Energy associated with the meridional circulation and temperature field is much smaller than that associated with the zonal mean zonal flow (Wallace

Corresponding author address: Dr. Matthew H. Hitchman, Department of Meteorology, University of Wisconsin–Madison, Madison, WI 53706.

1967). Since the mean state is observed to maintain thermal wind balance (Reed 1964; HL), temperature changes may be understood if zonal accelerations can be explained. The following terms in the zonal momentum equation may be estimated from LIMS data: observed zonal acceleration, advection by the mean meridional circulation, and wave driving by quasi-stationary planetary scale waves. In section 4 the residual of these terms is compared with wave driving calculated explicitly from observed Kelvin wave parameters. The upward flux of westerly momentum by Kelvin waves at 10 mb estimated from LIMS data is at least as large as previous estimates from radiosonde data. The highly derived nature of our calculations necessitates the use of caution. Nevertheless, the results of our comparison suggest that Kelvin wave driving is insufficient to account for the westerly phase of the stratopause SAO. The chief unbalanced term in the residual is the meridional advection of easterly angular momentum, which is largest in the lower mesosphere. A calculation of gravity wave driving based on Lindzen's wave breaking parameterization and LIMS zonal winds suggests that small scale waves could satisfy the momentum budget. Since observations show that a wide spectrum of gravity waves is generated by tropical convection (Pfister et al. 1986), it is perhaps reasonable to expect that waves other than Kelvin waves 1–6 would be important.

2. Application of slowly-varying theory of internal gravity waves

a. Theory

Bursts of Kelvin wave activity were observed as separate upward propagating, slowly varying wave packets at zonal wavenumbers 1, 2 and 3. Since the meridional wind is zero for the equatorially-trapped atmospheric Kelvin wave, it may be regarded as a special kind of low frequency, two-dimensional internal gravity wave. Relations governing wave–mean flow interaction for internal gravity waves are given in Lindzen (1971) and Boyd (1978). The following treatment closely follows Coy (1983). Wave amplitude, zonal mean wind, density, and damping are assumed to vary much more slowly in space and time than the phase of an individual wave. This two-scaling approach is often referred to as the WKBJ method. It leads to a separation of the dependence of vertical and meridional structure on the Doppler-shifted zonal trace speed, $c_x - \bar{u}$. Given only observed temperatures, information about the relationship among Kelvin wave variables is required to estimate wave driving. The observed structure will be used to determine the validity of this approach. A list of symbols is given in the Appendix.

For $L_z \ll 2\pi H$, $L_z \ll L_u$, and $\tau \ll 2\pi\tau_D$ a plane wave solution is valid, and the eddy continuity, zonal momentum, and thermodynamic energy equations for a nearly hydrostatic wave ($L_z \ll L_x$) become

$$u_0 = -\frac{m}{k} w_0,\ h_0 = \frac{(\omega - \bar{u}k)}{k} u_0,\ h_0 = \frac{N^2}{(\omega - \bar{u}k)m} w_0,$$

where $(\ )_0$ indicates amplitude. These can be combined to give the dispersion relation

$$\omega - \bar{u}k = -\frac{Nk}{m} \quad \text{or} \quad L_z = \frac{2\pi}{N}\left(\frac{L_x}{\tau} - \bar{u}\right). \tag{2.1}$$

The zonal and vertical trace speeds (cf. Pedlosky 1979, p. 72) are $c_x = \omega/k$ and $c_z = \omega/m$. For $\omega > \bar{u}k$ and $m < 0$, phase propagates eastward and downward. The zonal and vertical group velocities, $\partial\omega/\partial k$ and $\partial\omega/\partial m$, are

$$G_x = \bar{u} - \frac{N}{m} = c_x \tag{2.2}$$

$$G_z = -\frac{Nk}{m|m|} = \frac{k}{N}(c_x - \bar{u})^2 = -c_z - \bar{u}\frac{L_z}{L_x}, \tag{2.3}$$

where $m < 0$ indicates eastward and upward energy propagation. The latitudinal scale of wave energy in the case of large Richardson number is

$$L_y = \left(\frac{c_x - \bar{u}}{\beta}\right)^{1/2}, \tag{2.4}$$

where $\beta = 2\Omega a$ (Lindzen 1971).

After the formation of a vertically propagating wave packet, ω and k do not change to first order. They become tracers of wave activity for the packet. Activity associated with higher zonal trace speeds or higher zonal wavenumbers travels upward faster. Since $L_z \ll L_x$ for Kelvin waves, wave energy traverses one vertical wavelength in about one wave period. As the wave activity propagates upward through westerly shear, L_z, G_z and L_y will decrease. In this slowly-varying theory, surfaces of constant phase are expected to pack closer together. The wave activity will not penetrate its critical level, where $c_x - \bar{u} \to 0$.

The kinetic plus potential energies in a Kelvin wave of frequency ω and wavenumber k is $E_\omega = [R/(HN)]^2(T'_\omega)^2$. Wave activity density (cf. Andrews et al. 1987, p. 131)

$$A_\omega = \left\langle \frac{\rho E}{c_x - \bar{u}} \right\rangle = \frac{\rho\left(\frac{R}{HN}\right)^2 \langle\overline{(T'_\omega)^2}\rangle}{\frac{2\pi a}{k^*\tau} - \bar{u}} \tag{2.5}$$

is conserved away from a source region unless the waves are damped:

$$\frac{\partial A_\omega}{\partial t} + \frac{\partial}{\partial z}(A_\omega G_z) = -\alpha A_\omega + S_\omega \tag{2.6}$$

where, from (2.3) and (2.5), the wave activity flux is

$$A_\omega G_z = \rho\left(\frac{R}{HN}\right)^2 \cdot \frac{1}{N}\left(\frac{2\pi}{\tau} - \frac{k^*\bar{u}}{a}\right)\langle\overline{(T'_\omega)^2}\rangle, \quad (2.7)$$

$k^* = ka$, and the angled brackets denote a latitudinal average. In the transformed Eulerian mean zonal momentum equation (Andrews and McIntyre 1976; Edmon et al. 1980), the body force per unit mass due to Kelvin waves (for which $v' = 0$) is just the vertical convergence of total wave activity flux:

$$DF_K = -\frac{1}{\rho}\frac{\partial}{\partial z}\rho\langle\overline{u'w'}\rangle = \sum_{k^*=1}^{K} -\frac{1}{\rho}\frac{\partial}{\partial z}\int_0^\infty A_\omega G_z d\omega. \quad (2.8)$$

Under definition (2.7) the wave activity flux is upward, whereas the EP flux, $-\rho\overline{u'w'} = -AG_z$, is directed downward. It turns out that the Kelvin wave signal in the LIMS data is negligible for $k^* > 3$; $K = 3$ is sufficient.

Averaged over a long time period, a region with weak forcing and dissipation will tend to have height independent wave activity flux so that $A \sim G_z^{-1}$. Since G_z varies as $(c_x - \bar{u})^2$, A would vary as $(c_x - \bar{u})^{-2}$ in such a region. In this sense, time averaged wave activity density should increase with height in weakly dissipative westerly shear zones. As $(c_x - \bar{u})$ continues to decrease upward in westerly shear zones, dissipation eventually dominates, and A begins to decrease with height. This pattern of vertical variation gives an impression of accumulation of wave activity in westerly shear zones.

Over the lifetime of a wave packet, wave activity flux convergence will be balanced by damping (2.6), so that an alternative estimate of the body force per unit mass is

$$DF_K = \sum_{k^*=1}^{3} \frac{\alpha}{\rho}\int_0^\infty A_\omega d\omega. \quad (2.9)$$

Since A is expected to accumulate in western shear, DF_K should be larger in westerly than in easterly shear. In steady state (2.6) suggests a vertical decay scale for wave activity flux:

$$H_p = \frac{G_z}{\alpha}. \quad (2.10)$$

This penetration scale is larger for waves with large zonal trace speeds, is smaller in westerlies, and gets very small near a critical level. Dunkerton (1979) gives an interesting theoretical discussion of the zonal trace speeds required to obtain zonal flow acceleration, assuming certain damping profiles.

b. *Application to data*

In employing satellite temperatures to estimate Kelvin wave driving, two major considerations arise. The first is whether to use daily mapped temperatures or values which have been spectrally decomposed into frequencies. Spectral filtering can substantially reduce amplitudes. A finite wave packet must be represented by a wide range of frequencies. Kelvin wave amplitudes are underestimated when integrated over a finite band of frequencies. For example, during January–February typical wave one amplitudes near 0.7 mb are ~5 K in the daily data but are <1 K when integrated over the spectral band 6.7–8.6 days (Salby et al. 1984; Chi-Rong Sun, personal communication). Each zonal wavenumber propagates upward as a separate wave packet, so we choose to calculate wave driving for each wavenumber separately, with daily values effectively representing integrals over all frequencies:

$$\int_0^\infty A_\omega d\omega = \frac{\rho\left(\frac{R}{HN}\right)^2\langle\overline{(T')^2}\rangle}{\frac{2\pi a}{k^*\tau} - \bar{u}}. \quad (2.11)$$

Only the dominant values of τ, to be determined in section 3, are observable in daily data. These values of τ for a given k^* and pressure level, are used in conjunction with daily values of $\bar{u}$ and $\overline{(T')^2}$, to estimate wave activity density, wave activity flux, and body force per unit mass via (2.8) and (2.9). The wave packets we will refer to are temporal wave packets separated by zonal wavenumber.

With this approach, however, there is the danger of overestimating Kelvin wave amplitudes if some of the daily temperature variance is due to other kinds of waves. Ideally, it would be useful to numerically separate Kelvin waves from Rossby waves and layered structures (Hitchman et al. 1987). In all separation methods tried, coincidence of several different wave types led to patchy separation and artificial discontinuities in wave fluxes. Daily xz, yz and tz sections of wave temperature coefficients have been used to diagnose wave types and ascertain which portions are actually due to Kelvin waves. (The regions where other waves contribute to wave activity are flagged in Fig. 5.)

The second consideration arises from latitudinal scale expansion and contraction in vertical shear (2.4), a phenomenon which has been documented in observations (Salby et al. 1984). From theory (Lindzen 1971) one expects that

$$\overline{(T')^2}(y) \propto \exp\left[-\frac{1}{2}\left(\frac{y}{L_y}\right)^2\right]. \quad (2.12)$$

To estimate the momentum budget it is necessary to choose limits for latitudinal averaging, $\langle(T')^2\rangle$. If a band were chosen to be wide enough to capture most of the Kelvin wave activity as L_y varies, the SAO itself would be obscured in the averaging process. If the budget were performed only at the equator, $(T')^2$ would vary in altitude from a dilution or concentration of wave activity due to latitudinal scale expansion, giving

a spurious variation in DF_K. We restrict our comparison to the band 10°S–10°N. In westerly vertical shear wave activity would converge into this band from the subtropics. This would effectively diminish the estimated upward decrease in wave activity flux due to absorption, so that DF_K would be underestimated in (2.8). An overestimate would be obtained in easterly shear. We correct for this as follows. For $\bar{u} = 0$ and the observed range of wave trace speeds, the fraction of the total Kelvin wave activity in the 10°S–10°N belt estimated from (2.4) and (2.12) is 50%–80%. The global average of $(T')^2$ at a given level will be independent of L_y. This suggests application of an expansion-contraction correction factor $[(c_x - \bar{u})/c_x]^{1/2}$ relative to the reference state $\bar{u} = 0$. We apply this to the ~40% of wave activity that may focus into or defocus out of the band 10°S–10°N. In (2.11) we use

$$\langle\overline{(T')^2}\rangle\left[0.6 + 0.4\left(\frac{c_x - \bar{u}}{c_x}\right)^{1/2}\right], \qquad (2.13)$$

where $\langle\overline{(T')^2}\rangle$ is the mean of $\frac{1}{2}(a^2 + b^2)$ for the latitudes 8°S, 4°S, 0°N, 4°N, 8°N and a and b are the cosine and sine coefficients for the particular wavenumber. In westerly shear the empirical correction in brackets in (2.13) leads to an *increase* in the estimates of DF_K by ~30%.

c. *Effects of zonal flow acceleration*

In the absence of vertical wind shear, damping will cause high frequency waves to dominate at higher altitudes, with dominant frequency increasing smoothly with increasing altitude (Coy and Hitchman 1984). There is a pronounced increase in the dominant frequency of a wave packet when it emerges from a westerly shear layer. Salby et al. (1984) have delineated separate modes of increasing frequency at increasing altitude in their spectral analyses. Such shifts are also seen in the GCM results of Hayashi et al. (1984), although these shifts are not as pronounced as in the data, probably because equatorial wind variations in the model are weaker. Wave activity at lower frequencies is preferentially absorbed in westerly shear layers, leaving a higher dominant frequency at higher levels (Coy and Hitchman 1984; Garcia and Salby 1987).

Zonal flow acceleration in westerly shear layers could also contribute to such a shift. From conservation of wave crests, $(\partial\omega/\partial z) + (\partial m/\partial t) = 0$. Using (2.1) and (2.3),

$$\frac{dc_x}{dt} = \frac{\partial c_x}{\partial t} + G_z\frac{\partial c_x}{\partial z} = \frac{\partial \bar{u}}{\partial t}. \qquad (2.14)$$

If a wave packet spends 10 days traversing a westerly shear layer which is accelerating at 2 m s^{-1} per day, zonal trace speeds of the packet emerging from the layer will be 20 m s^{-1} larger. Fritts and Dunkerton (1984) and Tanaka (1986) showed that this effect can be quite large for gravity waves (cf. Tanaka's Fig. 5). Although τ can change by this mechanism, $(c_x - \bar{u})$ remains approximately constant for the packet, so that L_z, L_y, G_z, H_p, A and DF_K should remain unchanged. Wave activity may be expected to penetrate about the same distance whether or not the flow is accelerating.

3. Kelvin wave events

a. *Comparison with theory*

Figure 1 shows the time–height variation of temperature at 0°E over the equator due to waves one and two. The horizontal layered structures present in the mesosphere during November–January (for example, between 0.5 and 0.1 mb, 8–20 December in Fig. 1a; Hitchman et al. 1987) are very different from the downward propagating waves typified by the wave 2 packet in the lower stratosphere during November. Vertically propagating and quasi-stationary wave 3 disturbances also occur (Fig. 2). Temperature amplitudes decrease with increasing wavenumber, with no discernible wavelike features at zonal scales 4–6 (not shown). Random fluctuations smaller than ~1 K are present in Figs. 1 and 2, however most of the features can be ascribed to the presence of Kelvin waves, Rossby waves, or layered structures.

By comparing Figs. 1 and 2 with observed vertical shear (Fig. 3) it can be seen that westerly shear layers act like semi-permeable barriers to upward wave activity flux. After westerly shear is reduced in the 10–2 mb layer in mid-December, shorter slower Kelvin waves are observed to much higher altitudes.

Two selected days which further illustrate the appearance of Kelvin wave fields are shown in Fig. 4. Below the westerly shear layer near 5 mb (Fig. 3) the field is dominated by wave two on 14 November (Fig. 4a) and by wave one on 8 May (Fig. 4b), although there is still some power at other wavenumbers. In daily sequences of longitude–height sections (not shown) individual wave crests move eastward and downward. Due to their packet nature, waves fade in amplitude at lower altitudes while new ones form at the leading, upper edge.

Under the slowly-varying assumption (2.1) and (2.3) provide descriptions of two-dimensional internal gravity waves. We now determine the extent to which the observed waves obey these relations. Particular wave events of interest are tabulated in Table 1. The time–height sections were used to determine values of τ and L_z centered about each date-pressure level pair.

Wave periods in Table 1 fall into two groups: those occurring above strong westerly shear and those below. For wave one, the upper and lower waves have periods of ~4 days and ~6–9 days, although April and May are dominated by a still slower wave one, $\tau \sim 12$ days. For wave two the upper and lower waves have periods of ~4 days and ~6–7 days. These values agree quite well with those determined by Salby et al. (1984) using time spectra for the January–February period. In ad-

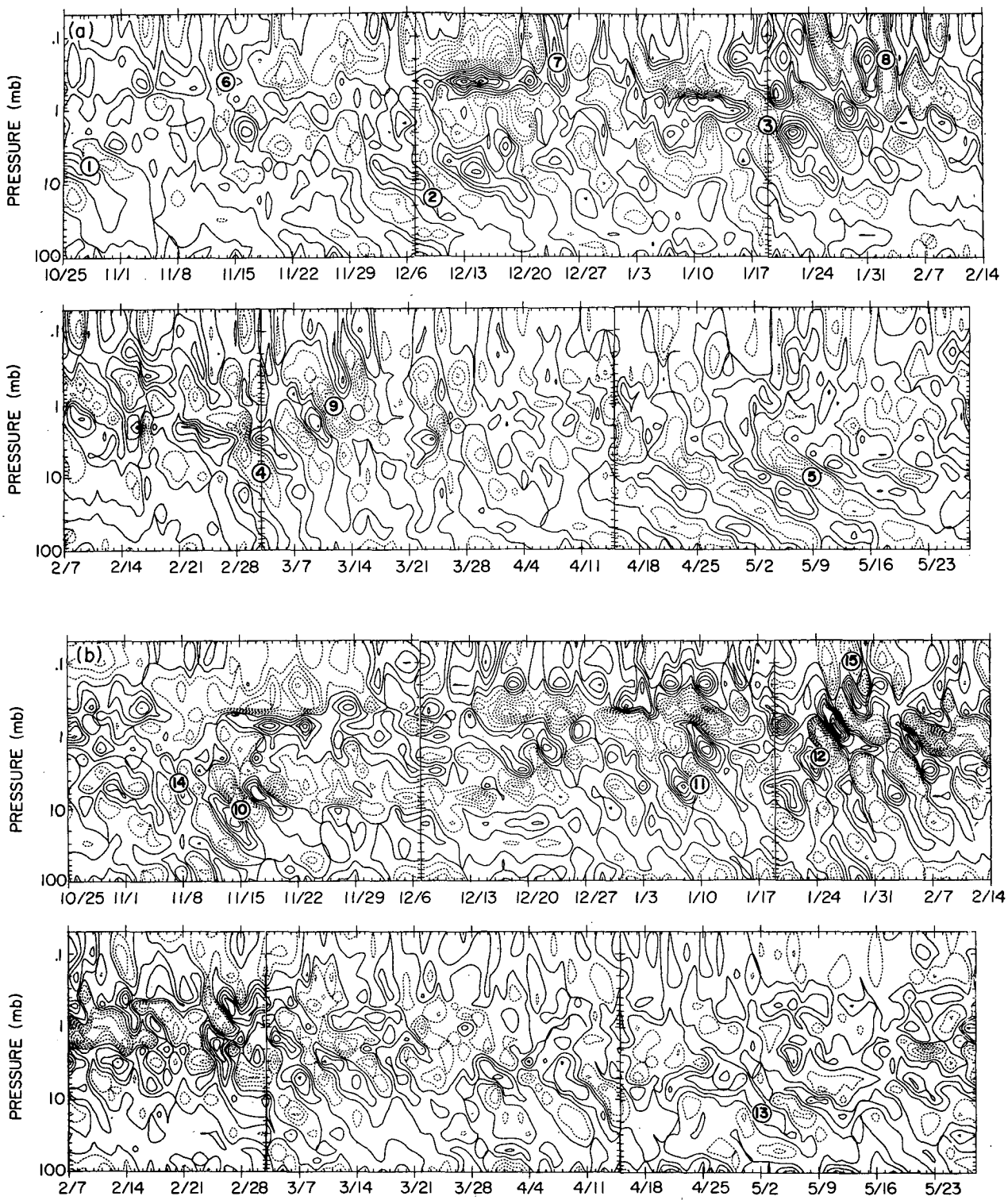

FIG. 1. Time–height sections of LIMS temperature cosine coefficient for (a) wave one (contour interval 1 K) and (b) wave two (contour interval 0.5 K), averaged in the latitude band 10°S–10°N, for the period 25 October 1978–28 May 1979. The week of 7–14 February is repeated for continuity.

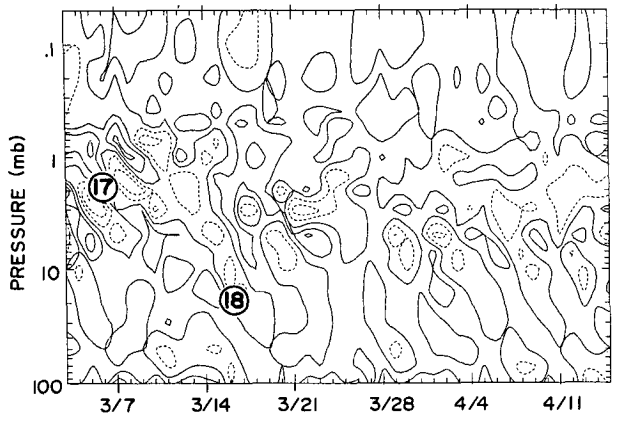

FIG. 2. As in Fig. 1 except for wave three during the period 3 March–15 April 1979. The contour interval is 0.5 K.

dition, wave 3 wave activity appears to be confined to levels below the strongest westerlies, with $\tau \sim 4$–5 days.

The dominant period observed for several days in a transient wave packet is the same as determined from spectral analysis. Temperature power is peaked rather narrowly in certain frequency bands (cf. Salby et al. 1984). Therefore, although other harmonics contribute to observed daily amplitudes, for purposes of calculating DF_K these amplitudes will be treated as corresponding to observed dominant periods.

In Table 1, $L_z \sim 16$–22 km for the slow wave one, 28–42 km for the fast wave one, 14–22 km for all wave two, and 13–18 km for wave three Kelvin waves. L_z does not appear to depend strongly on local values of $\bar{u}$. Even where waves are closer to a critical level (e.g., case 15) the vertical wavelength is not observed to shorten dramatically. This could be due in part to vertical resolution limitations in the LIMS data, although the shortest wavelengths listed in Table 1 are well above the resolution limit. Alternatively, this could be the result of the expected upward decrease in dominant period (τ^{dom}) through a westerly shear layer due to preferential absorption (section 2c). From (2.1),

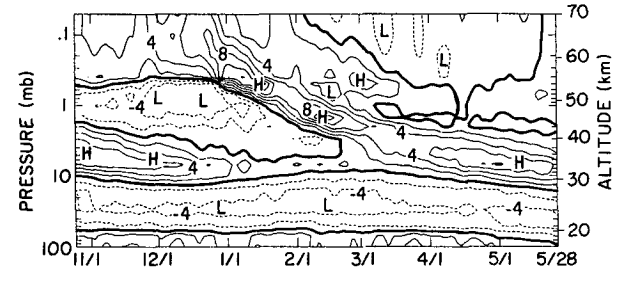

FIG. 3. Time–height section of vertical shear of the LIMS zonal mean zonal wind, averaged in the latitude band 10°S–10°N, for the period 25 October 1978–28 May 1979. The contour interval is 2 m s^{-1}/km.

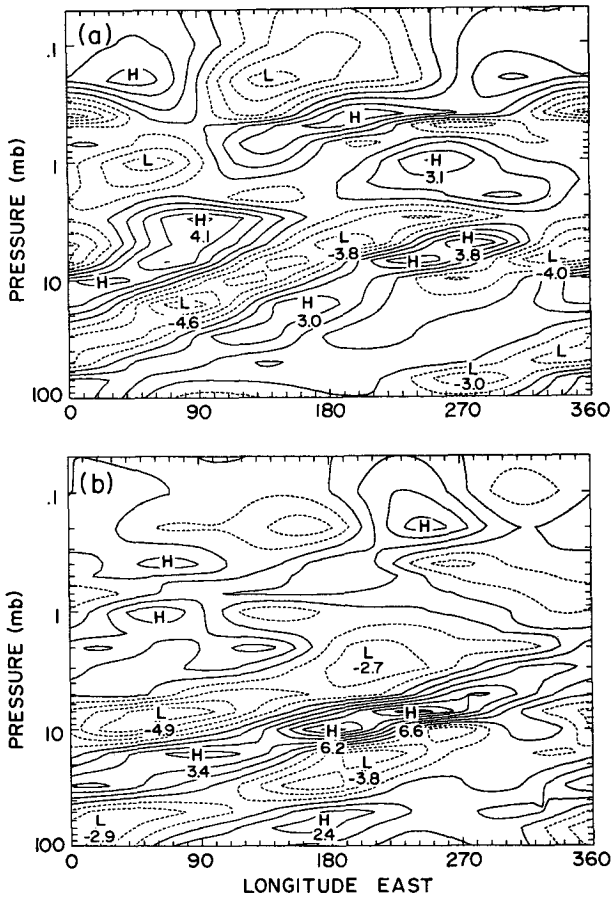

FIG. 4. Longitude–height sections of LIMS temperature on (a) 14 November 1978 and (b) 8 May 1979, averaged in the latitude band 5°S–5°N. Waves one, two and three are included in the analysis. The contour interval is 1 K.

$$\frac{\partial L_z^{\text{dom}}}{\partial z} \propto \frac{\partial c_x^{\text{dom}}}{\partial z} - \frac{\partial \bar{u}}{\partial z}, \tag{3.1}$$

so that L_z^{dom} will not decrease upward as rapidly in westerly shear if c_x^{dom} increases upward. Nevertheless, L_z does not appear to vary much in easterly shear either, where wave absorption is weak (e.g., compare Figs. 3 and 4). How valid is the WKBJ approximation? In the lower mesosphere $\tau_D \sim 2$ days (Leovy 1984) while $\tau \sim 4$ days. In the lower stratosphere in May $\tau_D \sim 10$ days and $\tau \sim 12$ days. Since $\tau \ll 2\pi\tau_D$, the slowly-varying assumption in time is generally a good one. On the other hand, the vertical "wavelength" of the SAO in $\bar{u}$ (Fig. 3) is $L_u \sim 30$–70 km. The slowly-varying assumption for vertical variations is expected to be less valid for the taller waves than for the shorter waves.

Observed values of L_z are compared with 'predicted' values, L_z^*, by using observed local values of $\bar{u}$, N, τ and L_x in (2.1). For cases 1–9 (wave one) the rms difference between L_z and L_z^* is 29% with a bias of +10% in the predicted mean value. For the eight cases involving waves two and three (excluding the near-critical

TABLE 1. Some Kelvin wave events during October 1978–May 1979. Wave period, vertical wavelength, and vertical group velocity were determined by using a straight-edge in the vicinity of the date–pressure level pair for the given zonal wavenumber. Observed zonal mean zonal wind and buoyancy frequency at these points are also given. Trace speeds are inferred. Predicted vertical wavelength, L_z^*, vertical group velocity, G_z^*, and penetration scale, H_p, are calculated from theory (see text). Observed vertical group velocity is omitted where estimation is difficult.

Case	Date	Level p (mb)	Wave-number k^*	Zonal wind $\bar{u}$ (m s^{-1})	Buoyancy frequency N (s^{-1})	Wave period τ (days)	Zonal trace speed c_x (m s^{-1})	Vertical trace speed c_z (km day^{-1})	Vertical wavelength L_z (km)	Predicted L_z^* (km)	Vertical group speed G_z (km day^{-1})	Predicted G_z^* (km day^{-1})	Penetration scale H_p (km)
1	10/28	5.0	1	10	0.021	9	51	−1.8	16	12	—	1.9	6
2	12/9	16.0	1	−25	0.021	9	51	−1.8	16	23	1.5	1.9	9
3	1/19	2.0	1	−40	0.022	6	75	−3.7	22	33	2.0	3.7	9
4	3/3	10.0	1	−30	0.022	7	66	−3.1	22	27	2.5	3.7	16
5	5/9	10.0	1	−20	0.022	12	38	−1.3	16	16	1.5	1.9	8
6	11/14	0.4	1	10	0.016	4	115	−10.0	40	41	—	8.8	18
7	12/24	0.2	1	−20	0.017	4	115	−9.0	36	49	—	7.6	15
8	2/2	0.2	1	40	0.015	4	115	−10.0	42	32	—	9.1	18
9	3/12	1.0	1	15	0.019	5	92	−5.6	28	25	2.5	5.1	10
10	11/15	10.0	2	−20	0.021	6	38	−2.7	16	17	3.0	3.7	16
11	1/10	5.0	2	−20	0.022	6	38	−2.8	17	16	3.0	4.4	14
12	1/24	2.0	2	−40	0.022	6	38	−3.7	22	22	3.5	7.3	17
13	5/2	16.0	2	−30	0.022	7	33	−2.1	15	18	2.5	3.4	17
14	11/8	5.0	2	10	0.021	4	57	−3.5	14	14	—	2.8	10
15	1/28	0.1	2	50	0.016	4	57	−5.5	22	5	—	5.3	7
16	10/28	5.0	3	0	0.021	4	38	−3.7	13	11	—	3.7	12
17	3/6	2.0	3	0	0.022	4	38	−3.7	13	11	3.0	3.9	9
18	3/16	20.0	3	−30	0.022	5	31	−4.0	18	17	3.0	7.6	40

level case), the rms difference is only 7%, with bias −1%. The agreement with theory is very good for waves two and three, which are shorter, on average, than wave one Kelvin waves. If $\bar{u} = 0$ is used in (2.1), the rms difference falls to 8% for wave one. It is reasonable to expect that any wave which extends over a range in which the background state varies substantially will have a structure which is compatible with the average of the background state over that range. These results suggest that the WKBJ relation (2.1) could be applied even in situations where wave and mean flow vertical scales are similar, by using vertical means of N and $\bar{u}$.

Rough estimates of G_z from time–height sections, shown in Table 1, support the concept that the observed Kelvin waves are dispersive in zonal and vertical wavenumber. As expected from (2.3), for the same vertical scale, wave activity associated with a longer zonal scale travels upward more slowly than that associated with a shorter zonal scale (compare cases 2 and 10, 3 and 12, 5 and 13). This is an a posteriori justification for examining Kelvin wave packet propagation independently for each zonal wavenumber. For the same zonal scale, wave activity associated with taller, higher trace speed waves tends to travel upward faster (e.g., cases 12 and 13). "Predicted" values of G_z, using observed values of N and L_z in the first equality in (2.3), however, are generally larger than the rough estimates based on the observations. Observed downward trace speeds are closer in magnitude to predicted upward values of G_z. Table 1 shows that taller, higher frequency waves individually propagate downward more rapidly than shorter, lower frequency waves.

Also included in Table 1 are values of the penetration scale (2.10), where predicted values, G_z^*, are used, and the damping profile is taken to be

$$\alpha(z) = \begin{cases} (0.0135z - 0.175)\ \text{day}^{-1}, & 16 \leqslant z \leqslant 50\ \text{km} \\ 0.5\ \text{day}^{-1}, & z \geqslant 50\ \text{km}. \end{cases} \tag{3.2}$$

In (3.2) z in km above the ground gives α in units of per day. This profile is similar to Fels' (1982) result for $L_z = 15$ km and the "thin limit" of Wehrbein and Leovy (1982). For given k^* and τ, H_p is larger in the lower stratosphere, where damping is slower (cases 1 and 2). Since $G_z \propto (\omega - \bar{u}k)^2$, wave activity associated with shorter period waves penetrates to higher altitudes in one damping period (compare cases 4 and 5). The mean of these 18 values of H_p is 14 km.

In Table 1 $\bar{u}$ varies much more than τ or N. The constant $N = 0.02$ s^{-1} is used in calculating A and G_z, hence DF_K from (2.8) or (2.9). The following constant values of τ in days are chosen for use in these formulae: $\tau = 6$ for wave 2, $\tau = 5$ for wave 3, $\tau = 10$ for wave one at and below the 3 mb level, $\tau = 5$ above. A for wave one will have a discontinuous upward decrease at 3 mb. However, due to the dominance of $(T')^2$ and $\bar{u}$, this effect is not very noticeable in the results.

b. Bulk properties

Equatorial time–height sections of A/ρ for waves one, two, and three are shown in Fig. 5. If A were contoured instead, only phenomena at the lowest levels could be seen. Those regions determined by careful inspection of daily wave structure to be due even partly to Rossby wave or layered structures are flagged in Fig. 5. These time sections show succinctly that wave activity accumulates in westerly shear.

Wave activity flux density, is contoured for waves one, two, and three in Fig. 6. $AG_z \rightarrow 0$ at a critical line, which does occur for waves two and three where $c_x = 38$ and 31 m s^{-1}, respectively. Wave activity flux penetrates to higher altitudes in easterlies. The mean value of H_p from Table 1, ~14 km, is compatible with the upward decrease of AG_z in Fig. 6. It can be seen that most of the loss of wave activity flux occurs well below any critical level, suggesting that wave breaking is probably not as important as radiative damping.

Upward packet propagation can be traced readily back to the 70 mb level and source times can be estimated. These are shown as vertical arrows in Fig. 6. Wave one, two, and three bursts occur largely independently of one another. Not only does wave activity propagate independently for each zonal scale, Kelvin wave packets of different zonal scale appear to be forced separately. There are two distinct regimes of Kelvin wave activity. Before April a packet regime dominates. Thereafter wave one packets dominate, with pulses coming so close together that the flux may be characterized as a nearly continuous wave one regime, although wave two and three packets still occur.

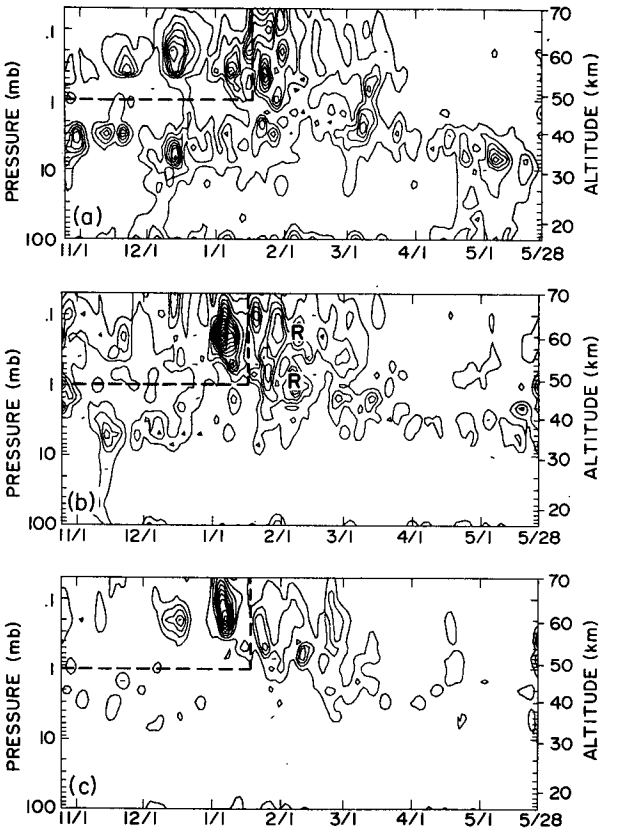

FIG. 5. Time–height sections of wave activity per unit mass, averaged in the latitude band 10°S–10°N, for the period 25 October 1978–28 May 1979, for waves (a) one, (b) two, and (c) three. The contour interval is 0.1 m s^{-1}. Prior to mid-January above the stratopause (region enclosed by the dash line box) layered structures contribute to the calculated wave activity. Regions partially due to Rossby waves of midlatitude origin are marked "R".

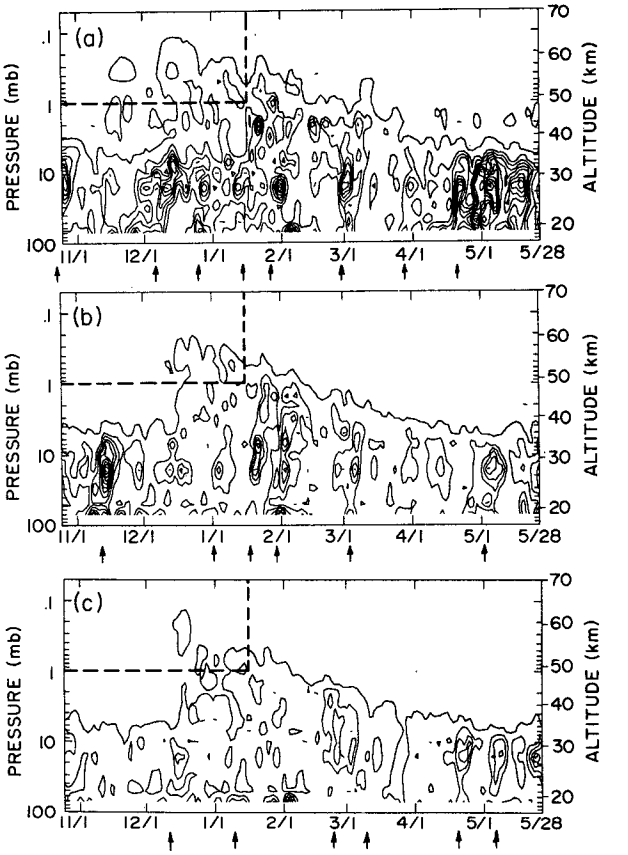

FIG. 6. As in Fig. 5 except for wave activity flux density. The contour interval is 2×10^{-5} Pa, starting at 0.5×10^{-5} Pa. Vertical arrows indicate source times for wave packets.

c. Implications for theories of Kelvin wave forcing

The range in horizontal scales of deep tropical convective systems is ~50–5000 km, corresponding to k^* ~ 4–400. Centers of convection occur near South America, Africa, and Indonesia. Tropical convection varies on hourly to interannual time scales (Murakami 1972; Orlanski and Polinski 1977; Liebmann and Hartmann 1982), with the power spectrum being generally red (Salby and Garcia 1987). Only a very small fraction of this immense energy is required to account for the observed Kelvin waves. There is no direct cor-

respondence, however, between the temporal and zonal scales of forcing and dominant Kelvin wave periods and zonal scales. Nevertheless, theoretical studies indicate that nascent wave structure can be influenced by the vertical scale of forcing and the forcing duration.

Dominance of the longest zonal scales may be due to a combination of preferred vertical and temporal scales. Chang (1976) predicted that the largest response will be for $L_z \sim 1.2\delta z$, where δz is the depth of the region of upward motion in the middle and upper troposphere ($\sim$10 km), and the variation in static stability is included. Taking $L_z \sim 12$ km, $\bar{u} = 0$, and $N = 0.02$ s^{-1} in (2.1), $c_x = 38$ m s^{-1}, which agrees well with lower stratospheric values in Table 1 (cases 5, 13 and 18). With the use of a numerical model, Holton (1973) found that stationary forcing with characteristic periods $\geq$ 10 days favors $k^* = 1$, while forcing with periods $\sim$4–10 days favors $k^* = 2$. Thus the lowest zonal wavenumbers will be preferentially excited by cloud systems which vary on time scales of 1–2 weeks. These earlier studies have been substantiated by the recent detailed work of Salby and Garcia (1987) and Garcia and Salby (1987), in which tropical convection is represented by stochastic processes in space and time. The vertical scale discrimination is found to be insensitive to variations in the heating distribution. Daily fluctuations tend to produce a response at Kelvin wave periods.

The observed dominance of $k^* = 1$, 2 or 3 at a given time (Fig. 6) may be due to the degree of transience in convective systems. Transient convective systems may be expected to excite a range of τ and L_z, with short slow waves masking the presence of tall fast waves in the lower stratosphere and the faster ones emerging at higher levels due to more successful penetration of westerly shear layers. The degree of separation in dominant frequency between lower and upper levels is probably related to the depth of the layer of westerly shear through which the wave activity ascends.

Another possible explanation of the observation that the dominant zonal scale differs from event to event is that the spatial pattern of forcing differs. For example, strong convection over Indonesia alone may preferentially excite wave one Kelvin waves. If convection strengthened over South America and Indonesia at the same time, perhaps wave two would be preferentially excited.

The switch from "packet" to "continuous" regimes at the end of March (Fig. 6) coincides with the transition from Northern Hemisphere winter to equinoctial conditions. It is quite common during the northern winter for surges of cold air to penetrate into the subtropics. These events are well-correlated with increased tropical cloud activity (Chang and Lau 1980). The average number of storms per month over the East China Sea is $\sim$6 from November through March, but drops rapidly to $\sim$1 per month by August (Hanson and Long 1985). The influence of midlatitude systems on tropical convection, with power peaked near one week, may explain the packet mode which prevailed during the northern winter 1978/79. As this influence fades during April, forcing may be expected to be more constant in time, with a continuous wave one preferred.

d. Estimation of errors

The error in calculating A due to the use of constant values of τ is estimated to be $\leq$30%, while errors in employing WKBJ theory are probably quite small for waves two and three and are estimated to be $\leq$30% for wave one. The primary factors contributing to DF_K in (2.8) are vertical changes in $\bar{u}$ and $\overline{(T')^2}$. Errors in $\bar{u}$ are less than 30% (HL). The error associated with $\overline{(T')^2}$, where $T' = T_a + T_e$, is $2(T_e/T_a) + (T_e/T_a)^2$. Taking $T_e = 0.5$ K as data precision and $T_a = 3$ K as a typical wave amplitude yields an error of $\sim$35%.

Our estimates may be biased on the low side if the apparent absence of wavelength shortening in westerly shear zones is a resolution effect, so that there is significant energy at unobserved higher vertical wavenumbers in these regions. Because the observed waves are well above the LIMS resolution limit, this is unlikely. On the other hand, two aspects of this analysis tend to bias the estimates upward: the attribution of all the temperature fluctuation energy to the Kelvin waves and the use of the LIMS IV dataset. Comparisons with rockets show that thermal fluctuations in the rocket data which yield vertical shear layers thicker than 7 km tend to be reproduced with equal or slightly greater amplitude in the LIMS IV dataset (cf. HL).

The time mean values of AG_z at 10 mb for waves one, two and three are 3.4, 1.9 and 1.3 in units of 10^{-5} Pa, or 52%, 29% and 19% of the total. Extrapolation to higher wavenumbers assuming power law behavior suggests that more than 80% of the upward momentum flux is due to the first three zonal wavenumbers. At 10 mb the sum of the time mean values of $\overline{u'w'}$ for all of the observed zonal waves is $\sim$0.006 m^2s^{-2}. Kousky and Wallace (1971) determined that at 32 mb $\overline{u'w'}$ $\sim$ 0.002 m^2s^{-2} during periods of strong Kelvin wave activity (QBO easterlies below 32 mb). Although Fig. 6 indicates that AG_z decreases upward, an upper bound on Kousky and Wallace's value extrapolated to 10 mb is obtained by assuming that AG_z is constant: $\sim$0.006 m^2s^{-2}. The 12 year average 50 mb value of 0.0003 m^2s^{-2} due to Angell et al. (1973), when extrapolated undiminished to 10 mb, becomes 0.0015 m^2s^{-2}. It appears that our current method, using LIMS temperatures, gives at least as much momentum flux due to Kelvin waves as previous estimates.

4. Wave driving

Equatorial time–height sections of daily values of the body force per unit mass due to Kelvin waves one–three, calculated from (2.8) and from (2.9), are shown

in Fig. 7. In the flux convergence formulation (Fig. 7a), DF_K is expected to be large in strong westerly shear where G_z decreases rapidly. The flux convergence representation does not depend on a steady-state assumption or damping profile. The damping parameterization (Fig. 7b) yields values which are ⅓ to ½ as large as values in Fig. 7a.

The locations of Kelvin wave driving in Fig. 7a coincide with descending westerly shear zones (Fig. 3) and regions of westerly acceleration. Observed zonal wind changes are smooth compared with episodes of Kelvin wave driving, despite the tendency of contributions due to packets of different characteristic zonal wavenumber to fill in gaps (compare Figs. 6 and 7a). The "spindown" time scale of mean meridional circulations driven by wave absorption is much longer than a week in the equatorial middle atmosphere (cf. Plumb and Bell 1982). Downward advection by this circulation will yield accelerations which vary less rapidly than wave driving events.

Several periods of strong intensification of westerly shear zones and acceleration are nevertheless noted: the initial formation of SAO westerlies in the lower mesosphere at the end of December, a strengthening of shear in early February, and again during April–May (Fig. 3). During April–May Kelvin wave driving is also enhanced. Near February 1 Kelvin wave packets are found (Fig. 6) and DF_K is somewhat larger. However, we believe that this event is also related to increased Rossby wave driving near the northern midlatitude stratopause, a result to be reported elsewhere. It is difficult to interpret mesospheric wave driving prior to mid-January due to the presence of layered structures. These structures occurred where the SAO westerlies formed in late December and may be partially responsible for increased vertical shears (cf. Fig. 8 of Hitchman et al. 1987). The reduction of SAO westerlies near 7 mb in late December is probably a more important factor: more Kelvin wave activity should reach the mesosphere beginning at that time. The same reasoning would apply to westerly gravity waves. In Fig. 8 we compare a LIMS-derived residual, the flux convergence form of Kelvin wave driving, and wave driving due to breaking gravity waves, all with six-day average values contoured in the same manner.

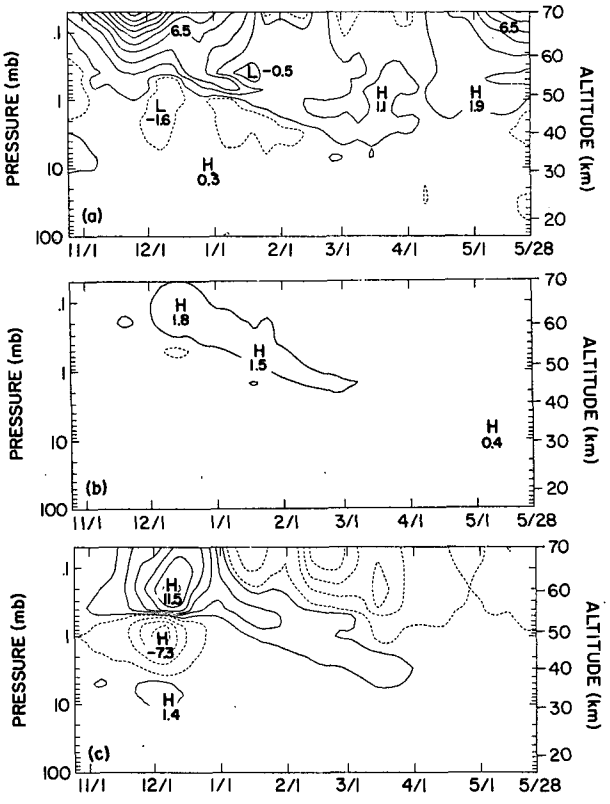

FIG. 8. Comparison of (a) the residual in the zonal momentum equation, as defined by (4.1), (b) as in Fig. 7a, and (c) wave driving due to gravity waves using Lindzen's parameterization (4.2), for the period 25 October 1978–28 May 1979, averaged in the band 10°S–10°N. Six day means are contoured with interval 2.0 m s^{-1}/day, beginning at ±0.5 m s^{-1}/day.

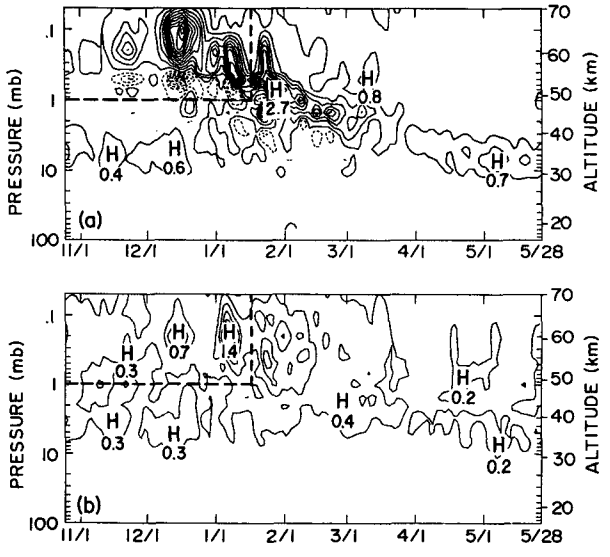

FIG. 7. Two estimates of the body force per unit mass due to Kelvin waves one–three using the parameterizations (a) (2.8) and (b) (2.9), for the period 25 October 1978–28 May 1979, averaged in the band 10°S–10°N. Daily values have been used. The contour interval is 0.2 m s^{-1}/day, beginning at ±0.1 m s^{-1}/day.

The residual is defined to be

$$DF_{\text{res}} \equiv \frac{\partial \bar{u}}{\partial t} + \bar{w}^* \frac{\partial \bar{u}}{\partial z} + \bar{v}^* \left(\frac{\partial \bar{u}}{\partial y} - f \right) - DF_{qs}, \quad (4.1)$$

where DF_{qs} is due to quasi-stationary planetary scale waves (Hitchman et al. 1987). Here $\partial\bar{u}/\partial y$ has been smoothed to insure that LIMS values are not larger than values calculated from rocket profiles. LIMS $\partial\bar{u}/\partial t$ and $\partial\bar{u}/\partial z$ values are within ~30% of values calculated from rocket data. In HL a detailed heating algorithm was used to estimate the residual circulation

as manifested in the temperature field. The magnitude of the residual circulation is quite comparable to other observational estimates (Crane et al. 1980; Solomon et al. 1986; Gille et al. 1987) and results from numerical models (e.g., Holton 1983). Over the equator DF_{qs} is quite small; the residual shown in Fig. 18c of HL, which excludes DF_{qs}, is very similar to Fig. 8a. Figure 8a shows that, in the lower mesosphere during November–January and April–May, easterly acceleration due to meridional advection of easterly angular momentum requires westerly wave driving to balance it. Near 2 mb during November–February the observed easterly acceleration is not completely accounted for by the other terms in DF_{res}. The observed westerly acceleration in the descending westerly shear zones is also unbalanced.

Wave driving due to breaking gravity waves (Fig. 8c) is estimated by using the parameterization of Lindzen (1981), modified by Holton (1982). Pfister et al. (1986) have observed a variety of gravity waves in the equatorial lower stratosphere in the presence of deep cumulus convection. Since gravity and Kelvin waves are forced by tropospheric convective systems, and are transmitted similarly, they may be expected to vary similarly in time. The arrows in Fig. 6 may well indicate times of enhanced gravity wave generation by tropical convection. If gravity waves are generated to a significant degree between large convective events they may contribute to the smoothness of the observed accelerations.

Gravity waves will break when their amplitudes are so large that they become convectively unstable. Above a wave's breaking level and below its critical level the mean flow will accelerate as the wave is absorbed. That is,

$$DF_g = \gamma(c_x - \bar{u})^2\left[\frac{(c_x - \bar{u})}{H} + 3\frac{\partial \bar{u}}{\partial z}\right] \qquad (4.2)$$

in the range of $z_b \leqslant z \leqslant z_c$, where

$$z_b = 3H \ln\left[\frac{|c_x - \bar{u}|}{\tilde{u}}\right] \qquad (4.3)$$

is the height of breaking above the formation level, and $\bar{u}$ is determined from LIMS observations. Zonal trace speeds and the parameters γ and $\tilde{u}$, which represent properties at 15 km, are specified in Table 2. To get gravity wave effects above the easterly and westerly winds of the quasi-biennial oscillation (~ -35 and $+20$ m s^{-1} at this time, HL), it was necessary to add waves with trace speeds of ± 40 m s^{-1}. The results depend sensitively on the assumed trace speeds for the fastest gravity waves, but the values $\pm$ 40 m s^{-1} are not completely arbitrary. As discussed in section 3c, forcing by deep convection will tend to produce internal gravity waves as well as Kelvin waves with trace speeds near 40 m s^{-1}. The values of $\tilde{u}$ and γ were chosen by modifying Holton's (1983) values to provide better agreement with DF_{res} in a latitude–altitude cross section for mid-December 1978. The algorithm was then applied using these values at all times. Profiles of DF_g were smoothed in the vertical to approximate various effects such as nonlinear interaction among waves and radiative damping.

TABLE 2. Gravity wave parameters.

c_x (m s^{-1})	γ ($\times 10^{-9}$ s-m^{-2})	$\tilde{n}$ (m s^{-1})
−40	0.5	1
−20	1.0	2
0	2.0	3
20	1.0	2
40	0.5	1

Although the pattern of DF_K in Fig. 7a is similar to DF_{res}, when the same time smoothing and contouring are used (Fig. 8b), two things become apparent. Firstly, there are regions where *easterly* accelerations are required. Secondly, DF_K is generally too small in regions where westerly accelerations are required. This deficit is most marked in the lower mesosphere. Some point comparisons in m s^{-1}/day for (DF_{res}, DF_K) are: (0.7, 0.1) at 7 mb on 1 November; (10.5, 0.4) at 0.1 mb on 1 December; (1.5, 1.0) at 1 mb on 1 February; (0.5, 0.2) at 5 mb on 15 March; and (0.4, 0.3) at 7 mb on 1 May.

It appears that westerly accelerations due to Kelvin waves account for a significant portion, perhaps 20%–70%, of required westerly accelerations in the stratosphere. Most of the Kelvin wave activity is absorbed in the stratosphere. Fast gravity waves, on the other hand, may be expected to penetrate to higher levels before being absorbed. The pattern of DF_g is quite similar to DF_{res} and magnitudes are sufficient in both the easterly and westerly sense. In the stratosphere both Kelvin and gravity waves are probably important, with Kelvin waves decreasing and gravity waves increasing in relative influence going upward into the mesosphere.

The influence of gravity waves is distinctly different at low latitudes compared with midlatitudes. In the tropics wind profiles are oscillatory in altitude and vertical shears are often more than 3 times as large as in midlatitudes (HL), reaching 8 m s^{-1}/km in the descending SAO westerly shear zone. The largest shears in Fig. 3 are westerly. This asymmetry is probably due to the associated meridional circulation: vertical convergence in westerly shear, divergence in easterly shear (HL). In the tall midlatitude jets, gravity waves with phase speeds in the direction of the zonal wind reach critical levels in the lower stratosphere, leaving waves with opposing phase speeds to decelerate the flow at upper levels. In the tropics the shear term in (4.2) dominates so that DF_g is the same sign as $\partial\bar{u}/\partial z$ (compare Figs. 3 and 8c). It can be shown that $AG_z \propto \rho(c_x - \bar{u})^3$ for saturated gravity waves. Where $L_u \ll 6\pi H$, there

will be wave activity flux convergence in westerly shear and divergence in easterly shear for saturated waves.

Some qualitative conclusions may be drawn from considering these results in view of the observed wind climatology (section 2, HL). Slower gravity waves may be expected to be absorbed in the equatorial lower stratosphere, strengthening flows that are present and influencing the QBO. Midlatitude Rossby and gravity wave driving will give rise to a summer to winter flow that increases upward, causing time mean equatorial easterlies near the stratopause. This layer of easterlies would tend to be strengthened by absorption of fast easterly gravity waves. Fast westerly gravity waves would be absorbed in the lower mesosphere, and could account for the observed time mean westerlies near 65 km. In addition, this would help accelerate the cross-equatorial flow in this layer, since the primary balance shown in Fig. 8 is

$$-(f-\bar{u}_y)\bar{v}^* \approx DF_g \qquad (4.4)$$

in the equatorial lower mesosphere.

The conclusion that gravity waves are important in this region has already been reached in studies with general circulation models (Hayashi et al. 1984; Kida 1985; Rind et al. 1988). Hayashi et al. found that, over the equator, vertical fluxes of easterly and westerly momentum due to gravity waves with periods 0.7–2 days (represented explicitly) are often greater than that due to Kelvin waves. A reasonable SAO was obtained by Rind et al., with parameterized fast gravity waves caused by tropical convection exerting a major influence. Dunkerton (1982) hypothesized that gravity waves are essential to the mesopause SAO. Our results suggest that they are also important to the stratopause SAO, with the relative importance increasing with altitude.

5. Summary

The LIMS experiment provided the first opportunity to document the three dimensional structure of Kelvin waves on a daily basis. It also provided the first opportunity to make quantitative estimates of the forcing of the mean state by these waves in the altitude range ~ 16–70 km. Their observed structure validates the use of the dispersion relation governing the behavior of two-dimensional internal gravity waves in estimating Kelvin wave driving. However, when the mean flow varies substantially over a wavelength the dispersion relation is less accurate.

It has been shown that Kelvin wave activity is dispersive in zonal wavelength as well as in wave period. A typical upward penetration scale for Kelvin wave activity is about two scale heights. Wave activity which emerges on the upper side of a westerly shear layer will have a shorter dominant period. Since the penetration scale is greater for higher frequency waves, this can be accounted for by preferential damping of the slower, shorter waves. Observed dominant vertical wavelengths do not appear to become very small approaching a critical level. This may be partly due to resolution effects. Alternatively, it may arise from preferential damping, or it may indicate that wave structure depends on a vertical mean of the background state.

It is useful to diagnose the behavior of Kelvin wave packets by calculating wave activity per unit mass and wave activity flux density. Wave activity is seen to accumulate in westerly shear. Most of the wave activity flux is lost via damping well below any critical level. The data suggest that a forcing regime, which is conducive to the formation of Kelvin wave packets of preferred characteristic zonal wavenumbers, prevails during the Northern Hemisphere winter. The forcing regime after the equinox tends to favor a more continuous zonal wave one. Data from other years would be required to verify this.

Neither rocket nor satellite soundings are ideally suited to detect small-scale gravity waves. Perhaps it is natural that previous explanations for the occurrence of westerlies over the equator were sought in the smooth robust signal of the planetary scale Kelvin wave. The accurate, high vertical resolution LIMS data, together with a detailed radiative heating algorithm, allow a relatively accurate estimation of the required momentum flux convergences as a residual in the zonal momentum equation. It appears that above ~30 km, planetary Kelvin waves 1–3 make a significant but decreasing contribution while the influence of smaller scale waves increases. This conclusion is nevertheless indirect. It will be very interesting to see if upcoming MST radar experiments yield gravity wave momentum flux convergences of the required magnitude.

Acknowledgments. We wish to thank Larry Coy for many helpful discussions, Rolando Garcia for comments on the manuscript, Chi-Rong Sun for sharing his time spectral computations, and Tim Dunkerton and Murry Salby for helpful reviews. This work is based in part on MHH's Ph.D. dissertation at the University of Washington. Our research was supported by NASA under Grant NAGW-471. MHH thanks the National Center for Atmospheric Research for support during revisions.

APPENDIX A

List of Symbols

$\overline{(\ )}, (\ )'$	Eulerian zonal mean and deviation
$\langle\ \rangle$	latitudinal average
$(\ )_\omega$	of a particular frequency
A	total wave action density for a particular zonal wavenumber
a	radius of the Earth
c_x, c_z	zonal and vertical trace speeds
DF_g	body force per unit mass due to gravity waves

DF_K	wave driving by Kelvin waves
DF_{qs}	wave driving by quasi-stationary waves
DF_{res}	residual wave driving
E	wave energy
f	Coriolis parameter
G_x, G_z	zonal and vertical group speeds
h	geopotential
H	scale height
H_p	vertical penetration scale
k, m	zonal and vertical wavenumbers
k^*	nondimensional zonal wavenumber
L_x, L_z	zonal and vertical wavelengths
L_y	meridional length scale
L_u	vertical 'wavelength' of zonal wind variation
N	buoyancy frequency
R	gas constant for dry air
S	source of wave activity
T, T_a, T_e	temperature, actual and estimated
$\tilde{u}$	gravity wave formation parameter
u, v, w	zonal, meridional and vertical wind components
$\bar{v}^*$, $\bar{w}^*$	Eulerian mean residual circulation
z_b, z_c	breaking and critical levels
α	damping rate
β	northward gradient of planetary vorticity
γ	gravity wave amplitude
ρ	basic state density
τ	wave period
τ_D	damping time scale
Ω	angular frequency of Earth's rotation
ω	wave frequency

REFERENCES

Andrews, D. G., and M. E. McIntyre, 1976: Planetary waves in horizontal and vertical shear: the generalized Eliassen-Palm relation and mean zonal acceleration. *J. Atmos. Sci.*, **33**, 2031–2048.

——, J. R. Holton and C. B. Leovy, 1987: *Middle Atmosphere Dynamics.* Academic Press, 489 pp.

Angell, J. K., G. F. Cotton and J. Korshover, 1973: A climatological analysis of oscillations of Kelvin wave period at 50 mb. *J. Atmos. Sci.*, **30**, 13–24.

Boyd, J. P., 1978: The effects of latitudinal shear on equatorial waves. Part I: Theory and methods. *J. Atmos. Sci.*, **35**, 2236–2258.

Chang, C.-P., 1976: Forcing of stratospheric Kelvin waves by tropospheric heat sources. *J. Atmos. Sci.*, **33**, 740–744.

——, and K. M. W. Lau, 1980: Northeasterly cold surges and near-equatorial disturbances over the winter MONEX area during December 1974. Part II: Planetary-scale aspects. *Mon. Wea. Rev.*, **108**, 298–312.

Coy, L., 1983: The vertical propagation of internal gravity waves in a compressible atmosphere. Ph.D. dissertation, University of Washington, 195 pp.

——, and M. H. Hitchman, 1984: Kelvin wave packets and flow acceleration: A comparison of modeling and observations. *J. Atmos. Sci.*, **41**, 1875–1880.

Crane, A. J., J. D. Haigh, J. A. Pyle and C. F. Rodgers, 1980: Mean meridional circulations of the stratosphere and mesosphere. *Pure Appl. Geophys.*, **118**, 307–328.

Dunkerton, T. J., 1979: On the role of the Kelvin wave in the westerly phase of the semiannual zonal wind oscillation. *J. Atmos. Sci.*, **36**, 32–41.

——, 1982: Theory of the mesopause semiannual oscillation. *J. Atmos. Sci.*, **39**, 2681–2690.

Edmon, H. J., B. J. Hoskins and M. E. McIntyre, 1980: Eliassen-Palm cross sections for the troposphere. *J. Atmos. Sci.*, **37**, 2600–2616.

Fels, S. B., 1982: A parameterization of scale-dependent radiative damping rates in the middle atmosphere. *J. Atmos. Sci.*, **39**, 1141–1152.

Fritts, D. C., and T. J. Dunkerton, 1984: A quasi-linear study of gravity-wave saturation and self-acceleration. *J. Atmos. Sci.*, **41**, 3272–3289.

Garcia, R. R., and M. L. Salby, 1987: Transient response to localized episodic heating in the tropics. Part II: Far-field behavior. *J. Atmos. Sci.*, **44**, 449–530.

Gille, J. C., and J. M. Russell III, 1984: The Limb Infrared Monitor of the Stratosphere (LIMS) experiment description, performance, and results. *J. Geophys. Res.*, **89**(D4), 5125–5140.

——, ——, P. L. Bailey, L. L. Gordley, E. E. Remsberg, J. H. Leinesh, W. G. Planet, F. B. House, L. V. Lyjak and S. A. Beck, 1984: Validation of temperature retrievals obtained by the Limb Infrared Monitor of the Stratosphere (LIMS) experiment on Nimbus 7. *J. Geophys. Res.*, **89**(D4), 5147–5160.

——, L. V. Lyjak and A. K. Smith, 1987: The global residual mean circulation in the middle atmosphere for the Northern winter period. *J. Atmos. Sci.*, **44**, 1437–1452.

Hamilton, K., 1982: Rocketsonde observations of the mesospheric semiannual oscillation at Kwajalein. *Atmos.-Ocean*, **20**, 281–286.

Hanson, H. P., and B. Long, 1985: Climatology of cyclogenesis over the East China Sea. *Mon. Wea. Rev.*, **113**, 697–707.

Hayashi, Y., D. G. Golder and J. D. Mahlman, 1984: Stratospheric and mesospheric Kelvin waves simulated by the GFDL "SKYHI" general circulation model. *J. Atmos. Sci.*, **41**, 1971–1984.

Hirota, I., 1978: Equatorial waves in the upper stratosphere and mesosphere in relation to the semiannual oscillation of the zonal wind. *J. Atmos. Sci.*, **35**, 714–722.

Hitchman, M. H., and C. B. Leovy, 1986: Evolution of the zonal mean state in the equatorial middle atmosphere during October 1978–May 1979. *J. Atmos. Sci.*, **43**, 3159–3176.

——, ——, J. C. Gille and P. L. Bailey, 1987: Quasi-stationary zonally asymmetric circulations in the equatorial lower mesosphere. *J. Atmos. Sci.*, **44**, 2219–2236.

Holton, J. R., 1973: On the frequency distribution of atmospheric Kelvin waves. *J. Atmos. Sci.*, **30**, 499–501.

——, 1982: The role of gravity wave induced drag and diffusion in the momentum budget of the mesosphere. *J. Atmos. Sci.*, **39**, 791–799.

——, 1983: The influence of gravity wave breaking on the general circulation of the middle atmosphere. *J. Atmos. Sci.*, **40**, 2497–2507.

——, and R. S. Lindzen, 1968: A note on "Kelvin" waves in the atmosphere. *Mon. Wea. Rev.*, **96**, 385–386.

Kida, H., 1985: A numerical experiment on the general circulation of the middle atmosphere with a three-dimensional model explicitly representing internal gravity waves and their breaking. *Pure Appl. Geophys.*, **122**, 731–746.

Kousky, V. E., and J. M. Wallace, 1971: On the interaction of Kelvin waves and the mean zonal flow. *J. Atmos. Sci.*, **28**, 162–169.

Leovy, C. B., 1984: Infrared radiative exchange in the middle atmosphere in the 15 micron band of carbon dioxide. *Dynamics of the Middle Atmosphere*, Terra Scientific, 355–366.

Liebmann, B., and D. L. Hartmann, 1982: Interannual variations of outgoing IR associated with tropical circulation changes during 1974–78. *J. Atmos. Sci.*, **39**, 1153–1162.

Lindzen, R. S., 1971: Equatorial planetary waves in shear: Part I. *J. Atmos. Sci.*, **28**, 609–622.

——, 1981: Turbulence and stress due to gravity wave and tidal breakdown. *J. Geophys. Res.*, **86**, 9707–9714.

Murakami, T., 1972: Equatorial stratospheric waves induced by diabatic heat sources. *J. Atmos. Sci.*, **29**, 1129–1137.

Orlanski, I., and L. J. Polinsky, 1977: Spectral distribution of cloud cover over Africa. *J. Meteor. Soc. Japan,* **55,** 483–493.

Pedlosky, J., 1979: *Geophysical Fluid Dynamics.* Springer-Verlag, 624 pp.

Pfister, L., W. Starr, R. Craig, M. Loewenstein and M. Legg, 1986: Small-scale motions observed by aircraft in the tropical lower stratosphere: evidence for mixing and its relationship to large-scale flows. *J. Atmos. Sci.,* **43,** 3210–3225.

Plumb, R. A., and R. C. Bell, 1982: A model of the quasi-biennial oscillation on an equatorial beta-plane. *Quart. J. Roy. Meteor. Soc.,* **108,** 335–352.

Reed, R. J., 1964: A tentative model of the 26-month oscillation in tropical latitudes. *Quart. J. Roy. Meteor. Soc.,* **90,** 441–446.

Rind, D., R. Suozzo, N. K. Balachandran, A. Lacis and G. Russell, 1988: The GISS global climate/middle atmosphere model with parameterized gravity wave drag. *J. Atmos. Sci.,* **45,** 371–386.

Salby, M. L., and R. R. Garcia, 1987: Transient response to localized episodic heating in the tropics. Part I: Excitation and short-time near-field behavior. *J. Atmos. Sci.,* **44,** 458–498.

——, D. L. Hartmann, P. L. Bailey and J. C. Gille, 1984: Evidence for equatorial Kelvin modes in Nimbus 7 LIMS. *J. Atmos. Sci.,* **40,** 220–235.

Solomon, S., J. T. Kiehl, R. R. Garcia and W. Grose, 1986: Tracer transport by the diabatic circulation deduced from satellite observations. *J. Atmos. Sci.,* **43,** 1603–1617.

Tanaka, H., 1986: A slowly varying model of the lower stratospheric zonal wind minimum by mesoscale mountain breakdown. *J. Atmos. Sci.,* **43,** 1881–1892.

Wallace, J. M., 1967: A note on the role of radiation in the biennial oscillation. *J. Atmos. Sci.,* **24,** 598–599.

——, and V. E. Kousky, 1968: Observational evidence of Kelvin waves in the tropical stratosphere. *J. Atmos. Sci.,* **25,** 900–907.

Wehrbein, W. M., and C. B. Leovy, 1982: An accurate radiative heating and cooling algorithm for use in a dynamical model of the middle atmosphere. *J. Atmos. Sci.,* **39,** 1532–1544.